2008

Carbonyl Sulfide (OCS): Large Scale Distributions Over North America During INTEX-NA and Relationship to CO2

Lambert Doezema
Loyola Marymount University, ldoezema@lmu.edu

Carbonyl sulfide (OCS): Large scale distributions over North America during INTEX-NA and relationship to CO_2.

Nicola J. Blake[1], Elliott Campbell[2], Stephanie A. Vay[3], Henry E. Fuelberg[4], L. Gregory Huey[5], Glen Sachse[3], Simone Meinardi[1], F. Sherwood Rowland[1], and Donald R. Blake[1]

1 Department of Chemistry, University of California, Irvine, CA (**nblake@uci.edu**, **drblake@uci.edu**, **smeinard@uci.edu**, rowland@uci.edu)

2 Center for Global and Regional Environmental Research, 401 Iowa Advanced Technology Labs, University of Iowa, Iowa City, IA 52242 (cae@engineering.uiowa.edu)

3 NASA Langley Research Center, Hampton, VA 23681-0001 (s.a.vay@larc.nasa.gov, g.w.sachse@larc.nasa.gov)

4 Department of Meteorology, Florida State University, Tallahassee, FL 32306, (fuelberg@huey.met.fsu.edu)

5 School of Earth & Atmospheric Sciences, Georgia Institute of Technology, Atlanta, GA 30332 (greg.huey@eas.gatech.edu)

Short Title: North American OCS sink

Index Terms: 0322 Constituent sources and sinks, 0345 Pollution--urban and regional, 0365 Troposphere--composition and chemistry, 0368 Troposphere--constituent transport and chemistry

Key Words: Carbonyl sulfide (OCS), Carbon Dioxide (CO_2), terrestrial sink, sources.

Abstract: An extensive set of carbonyl sulfide (OCS) observations were made as part of the NASA Intercontinental Chemical Transport Experiment - North America (INTEX-NA) study, flown from 1 July to 18 August 2004 mostly over the eastern United States and Canada. We use these data to show that summertime OCS mixing ratios at low altitude were dominated by a surface sink, and were highly correlated with CO_2. In marked contrast to the 2001 early springtime Transport and Chemical Evolution over the Pacific (TRACE-P) experiment, which sampled Asian outflow, anthropogenic OCS emissions were dominated by this draw-down, although evidence for local emissions were observed on some low altitude flight legs. The INTEX-NA observations are combined with the STEM regional atmospheric chemistry model for a top down validation of bottom up OCS surface fluxes. In preparation for 4 dimensional variational inversion, this manuscript summarizes INTEX-NA observations. The STEM model is applied to simulate OCS using the best available surface fluxes (1 degree, monthly, 8 sectors), fixed boundary conditions, and no chemical reactions. Initial STEM results suggest a 200% underestimation of the OCS sink.

1. Introduction

Sulfur dioxide (SO_2) is the major form of anthropogenic sulfur released to the troposphere. The reduced sulfur components, carbonyl sulfide (OCS) and carbon disulfide (CS_2), have large natural sources, but appreciable anthropogenic sources are also known [e.g., *Kettle et al*., 2002a, *Blake et al.,* 2004]. Both OCS and CS_2 are ultimately oxidized to SO_2 in the troposphere and/or stratosphere and may be relevant to

global climate change. The high tropospheric abundance (~500 pptv) and long tropospheric lifetime (2-7 years; *Xu et al.* [2002]) make OCS the major non-volcanic source of sulfur to the upper atmosphere. *Crutzen* [1976] hypothesized that atmospheric OCS is the primary source of the stratospheric sulfate aerosol layer, which is highly effective in reflecting incoming solar radiation back to space, enhancing the global albedo [*Charlson et al.,* 1990].

OCS is emitted to the atmosphere by the oceans, from biomass burning and through atmospheric oxidation of ocean carbon disulfide (CS_2) and dimethyl sulfide (DMS). Anthropogenic sources include coal combustion, aluminum production and sulfur recovery, and oxidation of anthropogenic CS_2 and DMS. Ice core and firn ice derived records suggest that human activities account for approximately 25 percent of modern atmospheric OCS levels [*Aydin et al.*, 2002]. Past and recent fluctuations are closely related to changing global anthropogenic sulfur emissions [*Montzka et al.*, 2004].

OCS is removed by terrestrial vegetation, soils, photolysis, and reactions with OH and O radicals [*Khalil and Rasmussen*, 1984; *Chin and Davis* 1993; *Andreae and Crutzen* 1997; *Watts*, 2000]. The magnitude and regional variation of the terrestrial vegetation sink has not been satisfactorily quantified [*Kettle et al*., 2002a]. OCS uptake by vegetation follows a common pathway through the stomata of leaves similar to that of CO_2 [*Goldan et al.,* 1988*; Sandoval-Soto et al.,* 2005]. However, because the OCS molecule is irreversibly consumed by photosynthesizing plants (in contrast to CO_2, which is also "exhaled" during respiration), OCS is thought to behave as a tracer of stomatal conductance and gross photosynthesis over vegetated land surfaces. Recent work by *Montzka and Tans* [2004] demonstrated that the amplitude of the seasonal cycles of OCS

and CO_2 are strongly correlated in the Northern Hemisphere mid- and high-latitudes. From this, *Montzka and Tans* inferred that the ratio of the uptake of OCS to CO_2 should reflect the ratio of photosynthesis to respiration. Thus, it is anticipated that OCS will provide insight into the mechanisms that control CO_2 sinks, improve the current systematic error in the simulated seasonal flux cycle of the CO_2 and to better understand the overall carbon cycle [*Montzka and Tans,* 2004; *Blake et al.,* 2005, *Gausepohl et al.,* 2006]

Experiment

During July and August 2004, observations of OCS and other species were made from the NASA DC-8 aircraft during the day-time over North America for Intercontinental Chemical Transport Experiment - North America (INTEX-NA). A major objective of INTEX-NA is to elucidate the sources, transport, and chemical evolution of air masses on transcontinental/intercontinental scales and their impact on air quality and climate. A particular focus for this study is the quantification and characterization of the inflow and outflow of pollution over North America.

Whole air samples were collected at a frequency of 1 to 5 minutes and analyzed in the UCI laboratory utilizing gas chromatography. The sampling and analytical equipment and procedures were almost identical to those employed by *Blake et al.* [2004] and *Colman et al*. [2001]. A short description follows. Air was collected in evacuated two-liter stainless steel canisters aboard the DC-8 and pressurized with a stainless steel (grease free) bellows pump. The canisters were analyzed in the Blake-Rowland laboratory at the University of California, Irvine (UCI), typically within one week of

sample collection. For analysis, cryogenically pre-concentrated sample was partitioned into five different streams, with each stream sent to one of five column-detector combinations optimized for nonmethane hydrocarbons, halocarbons [*Blake et al.,* 2003, *Colman et al.*, 2001]) and sulfur gases [*Blake et al.*, 2004]. The OCS calibration was performed by reference to a commercial standard (Scott Marrin).

The measurement precision for OCS was 5% with a detection limit better than 20 pptv. OCS was always present above its detection limit.

High precision in situ measurements of carbon dioxide (CO_2) were made on the DC-8 by a modified Li-COR model 6252 infrared gas analyzer having an accuracy and precision of 0.25 ppmv and 0.07 ppmv, respectively [*Vay et al.,* 1999].

Observations

INTEX-NA comprised 17 science flights during which a total of 2924 whole air samples were collected, covering an area from the Eastern Pacific to the Western Atlantic US. The Eastern US was the principal focus (Figure 1). The UC Irvine analysis quantified more than 50 different trace gases, including NMHCs, halocarbons and alkyl nitrates. However, this manuscript focuses on the observations of OCS and its relationship to CO_2 during INTEX-NA, with comparison to the Transport and Chemical Evolution over the Pacific (TRACE-P) observations and initial modeling results.

Sinks

The INTEX-NA observations, shown as averaged 1x1° grid squares (Figure 2). reveal that the lowest mixing ratios of OCS were found at the lowest altitudes, with

higher mixing ratios aloft over the Western US. This pattern is almost identical to that for CO_2. A significant correlation between OCS and CO_2 exists, with an R^2 of 0.67 for all INTEX-NA OCS data vs. CO_2 (Figure 3). Stronger correlations are found for several individual flights, mostly flown over vegetated regions of the Eastern US (Table 1 and Figure 4). Flight 12, flown on July 20, 2004, had the highest R^2 value (0.92) for OCS vs. CO_2. This flight comprised 6 low altitude legs, three of which were over the North Atlantic and three over different areas of the Eastern US (Figure 5). The low altitude legs flown over the ocean showed no significant drawdown (or obvious large enhancement) of either OCS or CO_2 (Figure 6). However, all three legs flown in the continental boundary layer (CBL) showed significant draw-down of both gases (Figure 6).

According to backwards trajectories and adjoint-derived influence regions (not shown), the air mass sampled over the ocean had spent at least several days in the marine boundary layer (Figure 7), while the air intercepted in the CBL had spent several days at low altitudes over vegetated continental regions of the US and Canada (Figure 8). Therefore, the Flight 12 data serves to illustrate the contrast between the strong sink of OCS and CO_2 at low altitudes for air with a history of terrestrial influence, compared to air masses with principally oceanic influence.

Comparison with TRACE-P

Because TRACE-P was flown in the Asian 2001 spring season, OCS soil and vegetation sinks were expected to be near seasonal lows [*Kettle et al.,* 2002b]. For TRACE-P, over the Western Pacific, OCS mixing ratios were enhanced by at least 10% in samples collected below 2 km altitude, compared to those collected at 8-10 km (Figure

9a). Similarly, strong gradients were observed for the anthropogenic tracer gas tetrachloroethene (C_2Cl_4) (Figure 9d and *Blake et al.* [2003, 2004]) and combustion marker CO (Figure 9b), suggesting that boundary layer levels of OCS may have been strongly influenced by continental anthropogenic sources during TRACE-P [*Blake et al.,* 2004]. Mean TRACE-P levels of OCS (as well as C_2Cl_4) over the Central and Eastern Pacific, at altitudes below about 4 km, were significantly lower than those over the Western Pacific (Figure 9). This was mainly the result of a diminished influence from continental sources [*Blake et al.,* 2004].

In contrast with the TRACE-P observations, the INTEX-NA OCS and CO_2 data show significant biogenic drawdown near the surface. A mean mixing ratio for OCS below 2 km of 0.41 ppbv accounts for a 10% depletion compared to a background value aloft of approximately 0.45 ppbv (Figure 9). The corresponding depletion for CO_2 was about 1.6%.

Sources

The high background concentrations of OCS and CO_2 originating from Asian and high latitude air masses contribute to high concentrations (> 0.5 ppbv) observed over the Pacific (Flight 3) and Atlantic (Flight 15) at high altitudes (8-10 km) (Figures 1 and 2). These high altitude enhancements have been linked to pollutant plumes originating from Asia. Like previous observations closer to the Asian continent [*Blake et al.,* 2004], plumes originating from parts of China associated with high levels of coal burning are particularly enhanced in OCS compared to CO.

Low altitude anthropogenic emission spikes of OCS and CO_2 are masked by the biosphere sink, which is co-located for OCS and CO_2 (Figure 10). These spikes become evident when if aligned with concurrent SO_2 observations (Figure 10). Figure 10 highlights a flight where the low altitude air originated over the Ohio River valley [*Hennigan et al.,* this issue]. The region bordering the Ohio River contains a large number of power plants that consume fossil fuels, primarily coal. Although this area only accounts for approximately two percent of the total U.S. surface area, it represents roughly 25 percent of U.S. point source emissions of SO_2. Unfortunately, we found few reported OCS emission factors for combustion representative of this area. The emission inventory of *Blake et al.* [2004] found only one reported measurement of OCS emissions from a coal fired powerplant, reporting an OCS/CO_2 ratio of 2.3 x10^{-6} (= 0.0049 g OCS kg^{-1} coal burned at the Cherokee Power Plant in Denver, CO) [*Khalil and Rasmussen*, 1984; *Chin and Davis*, 1993]. Taking data from the largest SO_2 spike observed during INTEX-NA, the enhancement ratio of OCS/CO_2 is approximately 6 x10^{-6} v/v. Another spike, which has enhancements for OCS, CO_2 and SO_2, yields an approximate OCS/CO_2 enhancement ratio 5 x10^{-6} v/v. These values are lower than the 9-24 x10^{-6} v/v range for OCS/CO_2 ratios in air masses originating over China and SE Asia during TRACE-P [*Blake et al., 2004*]. The likely course for this is the cleaner coal burned in the US and possible use of modern coal burning technology.

During flight 9 flown on 18 July, 2004 (Figure 1) a plume containing biomass burning emissions from Alaskan wildfires was sampled over the NW Atlantic, off the coast of Newfoundland. This plume had been transported rapidly across Canada in about 5 days. The OCS/CO_2 enhancement ratio was approximately 18 x10^{-6} v/v (R^2 = 0.70),

which is at the upper end of the range reported for SE Asian (mostly biomass burning) emissions [*Blake et al.,* 2004]. However, the corresponding value for the OCS/CO ratio is about 0.1 $x10^{-6}$ v/v, which is at the lower end of the observations for SE Asia, possibly reflecting an elevated summertime photochemical loss rate for CO relative to OCS.

STEM Model

The STEM (Sulfur Transport Eulerian Model) regional chemistry model [*Carmichael, et al.*, 2003a; *Carmichael, et al.*, 2003b] was used in preliminary simulations of OCS on the INTEX-NA domain, driven by the best available surface fluxes [*Kettle, et al.*, 2002], time invariant boundary conditions, and no chemical reactions. The model domain has a 60 km grid resolution and 21 sigma layers that extend from the surface up to 100 hPa.

The OCS surface fluxes have a 1 degree spatial resolution (model domain grid cell is 0.5 degree) and a monthly time resolution for the following eight flux components: terrestrial vegetation sink, soil sink, ocean source, anthropogenic source, oxidation of ocean CS_2, oxidation of ocean DMS, oxidation of anthropogenic CS_2, and oxidation of anthropogenic DMS [*Kettle, et al.*, 2002a] (for surface fluxes of these sectors for July see Figure 11). The terrestrial plant sink was dominant for the INTEX-NA period.

Three model runs are described in Table 2. Model run A incorporated only the plant component of the surface fluxes and fixed lateral and top boundary conditions of 0.45 ppbv OCS. Model run B incorporated all the flux components and showed results very similar to those obtained from model run A. Model run C used doubled plant fluxes

and increased boundary conditions of 0.48 ppbv OCS on the western lateral boundary (see below).

As seen in Figure 12a, model run C showed significant improvement over model run B for the model-to-observed correlation. The inferior model-to-observed correlation resulting from model run A indicates a tendency for over-prediction at low altitudes and under-prediction at high altitude (Figure 12b). This over-prediction may be due to an underestimation of the surface sink, while the under-prediction may be due to boundary conditions.

This western boundary OCS levels utilized in model run C was estimated based on data from the July 1^{rst} flight (Flight 3). The horizontal profile of OCS from this flight is shown in Figure 13 and the vertical distribution is highlighted on the distribution for all flights in Figure 14. The OCS concentration is 0.48 ± 0.01 ppbv for July 1^{rst} vs. 0.44 ± 0.04 ppbv for all flights (Figure 14), leading to an estimated OCS concentration of 0.48 ppbv at the Pacific boundary.

Defining the other lateral model domain boundaries is more complicated due to strong influence by terrestrial sinks. The OCS surface fluxes for Canada (Figure 11) indicate that the northern boundary will be highly varied. While these lateral boundaries may best be estimated as space varying time invariant surfaces [*Gerbig, et al.*, 2003], this initial approach employed a simple average of observations binned by longitude and altitude.

The top boundary condition was estimated from high altitude OCS data. The highest STEM vertical level over the ocean is centered at 13.1 km. The highest altitude for INTEX-NA OCS observations are at 11.9 km (Figure 9). Mean OCS observations

above 11km have a value of 0.46 ± 0.01 ppbv (Figure 9). This value is almost identical to the mean value observed for the similar altitude range over the Central Pacific during TRACE-P. The two data sets also exhibited similar low variability (Figure 9) with lack of an obvious horizontal, or even seasonal, trend. Thus, a value of 0.46 ppbv was adopted for the constant top boundary OCS concentration.

A time series of OCS concentrations compares the observed data to the values obtained from the model runs for the July 20th flight (Figure 15). None of the model runs capture the depth of the biosphere sink, even with a doubling of the biogenic sink as employed in model run C. The emissions and model resolutions are too coarse to show the low altitude, anthropogenic emission spikes. Anthropogenic input from Asia was also shown to influence this flight at high altitudes [*Liang et al.*, this issue], which may account for some of the high altitude (background) underestimation.

Conclusion and Next Steps

Unlike the net Asian OCS source investigated in TRACE-P during winter/spring [*Blake et al.*, 2004], the dominant terrestrial surface OCS flux in the North American summer is the vegetation sink. This sink works effectively and illustrates the large scale co-located summer draw-down of OCS and CO_2 and how terrestrial sinks dominate during this season at low altitudes over vegetated regions of North America. Initial STEM model results indicate that the current, proposed magnitude of the OCS surface sink may be underestimated by more than 200%.

Further development of the forward OCS model is planned, adding improved boundary conditions, emissions, and chemistry. The STEM adjoint model will then be

applied to obtain optimal estimates of OCS surface fluxes. In addition to a top down analysis of OCS, we are developing a simultaneous 4D-Var assimilation of OCS and CO_2 to exploit their high correlation. This work will combine the measurement and modeling of OCS and CO_2 and through the improved understanding of terrestrial biosphere sinks provide a novel approach to the study of the global carbon cycle.

Acknowledgments

We wish to thank Rowland/Blake group members Angela Baker, Barbara Barletta, Andreas Beyersdorf, Barbara Chisholm, Lambert Doezema, Kevin Gervais, Mike Kamboures, Gloria Liu, Brent Love, Jason Midyett, and Brian Novak for their outstanding contributions during the INTEX-NA mission, also the DC-8 crew the INTEX support staff. Thanks to Jack Dibb and Mads Andersen for manuscript suggestions. We gratefully acknowledge funding from the NASA Office of Earth Science Tropospheric Chemistry Program.

References

Andreae, M. O. and P. J. Crutzen, Atmospheric aerosols: biogeochemical sources and role in atmospheric chemistry; *Science*, 276, 1052-1056, 1997.

Aydin, M., W. J. De Bruyn, and E. S. Saltzman, "Preindustrial Atmospheric Carbonyl Sulfide (OCS) from an Antarctic Ice Core," *Geophys. Res. Lett.*, 10.1029/2002GL014796, 2002.

Blake, N. J., D. Streets, J.-H. Woo, I. Simpson, J. Green, S. Meinardi, et al., Carbonyl sulfide (OCS) and carbon disulfide (CS_2): Large scale distributions over the

Western Pacific and emissions from Asia during TRACE-P, *J. Geophys. Res.,* 109, D15S05, doi:10.1029/2003JD004259, 2004.

Blake, N J, Blake, D R, Baker, A, Beyersdorf, A, Doezema, L, Meinardi, S, Novak, B, Barletta, B, Midyett, J, Kamboures, M, Fuelberg, H E, Vay, S A, Rowland, F S, Spatial distributions, sources and sinks of methyl iodide, methyl chloride, methyl bromide, carbonyl sulfide, and other trace gases from observations over North America during INTEX-NA, Eos Trans. AGU, 86(52), Fall Meet. Suppl., Abstract A54C-05, 2005.

Carmichael, G. R., *et al.*, Computational aspects of chemical data assimilation into atmospheric models, in *Computational Science - Iccs 2003, Pt Iv, Proceedings*, edited, pp. 269-278, 2003a.

Carmichael, G. R., *et al.* Regional-scale chemical transport modeling in support of the analysis of observations obtained during the TRACE-P experiment, *J. Geophys. Res.-Atmospheres*, *108*, 2003b.

Charlson, R. J., J. Langner, and H. Rodhe, Sulphate aerosol and climate, *Nature*, 348, 22, 1990.

Chin, M. and D. D. Davis, Global sources and sinks of carbonyl sulfide and carbon disulfide and their distributions, *Global Biogeochem. Cycles,* 7(2), 321-37, 1993.

Colman, J. J., A. L. Swanson, S. Meinardi, B. C. Sive, D. R. Blake, and F. S. Rowland, Description of the analysis of a wide range of volatile organic compounds in whole air samples collected during PEM-Tropics A and B, *Anal. Chem.,* 73, 3723-3731, 2001.

Crutzen, P. J., The possible importance of OCS for the sulfate layer of the stratosphere, *Geophys. Res. Lett.*, 3, 73-76, 1976.

Gerbig, C. *et al*., Toward constraining regional-scale fluxes of CO_2 with atmospheric observations over a continent: 2. Analysis of COBRA data using a receptor-oriented framework, *Journal of Geophysical Research-Atmospheres*, *108*, 2003.

Gausepohl, S. C., A. S. Denning, J. Berry, S. Montzka, I. Baker, J. Kleist, Assessing the seasonal cycle of simulated photosynthesis using carbonyl sulfide (COS) at a continental mixed forest site, *Geophysical Research Abstracts*, Vol. 8, 05284, 2006

Goldan, P. D., Fall, R., Kuster, W. C., and Fehsenfeld, F. C.: Uptake of COS by growing vegetation – a major tropospheric sink, *J. Geophys. Res.-Atmospheres*, 93, D11, 14 186–14 192, 1988.

Hennigan, C., S. Sandholm, S. Kim, R. Stickel, L. G. Huey, R. Weber, Influence of Ohio River Valley Emissions on Fine Particle Sulfate Measured From Aircraft Over Large Regions of the Eastern U.S. and Canada During INTEX-NA, t*his issue.*

Kettle, A. J., et al., Global budget of atmospheric carbonyl sulfide: Temporal and spatial variations of the dominant sources and sinks, *J. Geophys. Res.-Atmospheres*, *107*, 2002a.

Kettle A. J., U. Kuhn, M. von Hobe, J. Kesselmeier, and M. O. Andreae, Comparing forward and inverse models to estimate the seasonal variation of hemisphere-integrated fluxes of carbonyl sulfide, *Atmospheric Chemistry & Physics*, 2:343-361, 2002b.

Khalil, M. A. K. and R. A. Rasmussen, Global sources, lifetimes and mass balances of carbonyl sulfide (OCS) and carbon disulfide (CS_2) in the earth's atmosphere, *Atmos. Environ.*, 18, 1805-1813, 1984.

Liang *et al.*, Summertime influence of Asian pollution in the free troposphere over North America, *this issue*.

Montzka, S. and P. Tans (2004), Can Carbonyl Sulfide Help Constrain Gross Vegetative Fluxes of Carbon Dioxide? *American Geophysical Union*, Fall Meeting 2004, abstract #B21E-04, 2004.

Sandoval-Soto, L., M. Stanimirov, M. von Hobe, V.Schmitt, J. Valdes, A. Wild and J. Kesselmeier Global uptake of carbonyl sulfide (COS) by terrestrial vegetation: Estimates corrected by deposition velocities normalized to the uptake of carbon dioxide (CO_2). *Biogeosciences*, 2, 125-132, 2005.

Vay, S. A., B. E. Anderson, T. J. Conway, G. W. Sachse, J. E. Collins, Jr., D. R. Blake, and D. J. Westberg, Airborne observations of the tropospheric CO_2 distribution and its controlling factors over the South Pacific Basin, *J. Geophys. Res.*, 104(D5), 5663-5676, 1999.

Watts, S.F., The mass budgets of carbonyl sulfide, dimethyl sulfide, carbon disulfide and hydrogen sulfide, *Atmos. Environ.*, 34, 761-779, 2000.

Xu, X., H. G. Bingemer and U. Schmidt, An empirical model for estimating the concentration of carbonyl sulfide in surface seawater from satellite measurements, *Geophys. Res. Lett*., 29 (9): 10.1029/2001GL014252, 2002.

Figures

Figure 1. Color-coded map of all DC-8 flight tracks for INTEX-NA superimposed on the STEM 60 km model domain grid.

Figure 2. Map of 1°x1° mean observed OCS concentrations for 3 altitude ranges for all INTEX-NA DC-8 flights (July and August 2004).

Figure 3. Correlation plot of OCS versus CO_2 for all for all INTEX-NA DC-8 flights (July and August 2004).

Figure 4. Correlation plots of R^2 values for CO_2 vs. OCS from Table 1 against CO_2 vs. OCS slopes and intercepts from Table 1.

Figure 5. Flight track with color-coded altitude for INTEX-NA DC-8 Flight 12, July 25, 2004. Small blue squares correspond to the positions of samples collected during the 6 boundary layer runs. Black numbers correspond to UTC hour.

Figure 6. Mixing ratios of OCS and CO_2 and altitude vs. UTC hour for INTEX-NA DC-8 Flight 12, July 25, 2004. Blue shading highlights marine boundary layer legs and green shading highlights continental boundary layer legs.

Figure 7. Backwards trajectory for the 1st low altitude leg during Flight 12, flown at about UTC hour 13:10 to 13:25.

Figure 8. Backwards trajectory for the 5th low altitude leg during Flight 12, flown at about UTC hour 19:45 to 20:15.

Figure 9. Mean (1-km increments) vertical profiles for a) OCS, b) CO, d) CO_2, d) C_2Cl_4. The mean values for INTEX-NA are compared to data collected over the Western Pacific

(<165°E) and Central/Eastern Pacific (165°E-230°E) during TRACE-P. Error bars represent 1 standard deviation from the mean.

Figure 10. Time series for INTEX-NA DC-8 observations of OCS, SO_2, and CO_2 during Flight 12, July 20, 2004.

Figure 11. OCS surface fluxes interpolated from *Kettle et al.* [2002] to the STEM 60 km model domain.

Figure 12a. OCS model vs. observed correlations for run B (blue) and run C (pink).

Figure 12b. OCS model vs. observed error for model run A.

Figure 12c. Model error (model vs. observations) for OCS and CO_2 for all INTEX-NA DC-8 flights.

Figure 13. Observed OCS mixing ratios for Flight 3, July 1, 2004

Figure 14. Observed OCS mixing ratios (blue) and 1-km mean values (black) for all flights for INTEX-NA. Samples from Flight 3, July 1, 2004, and 1-km mean values from this flight are highlighted in red.

Figure 15. OCS concentrations from observed data and model runs A, B and C (see Table 2) for INTEX-NA DC-8 flight, July 20, 2004 (Flight 10).

Tables

Table 1. Correlations of INTEX-NA observations of OCS and CO_2 for each INTEX-NA DC-8 flight, sorted by R^2.

Table 2. Preliminary STEM OCS simulation.

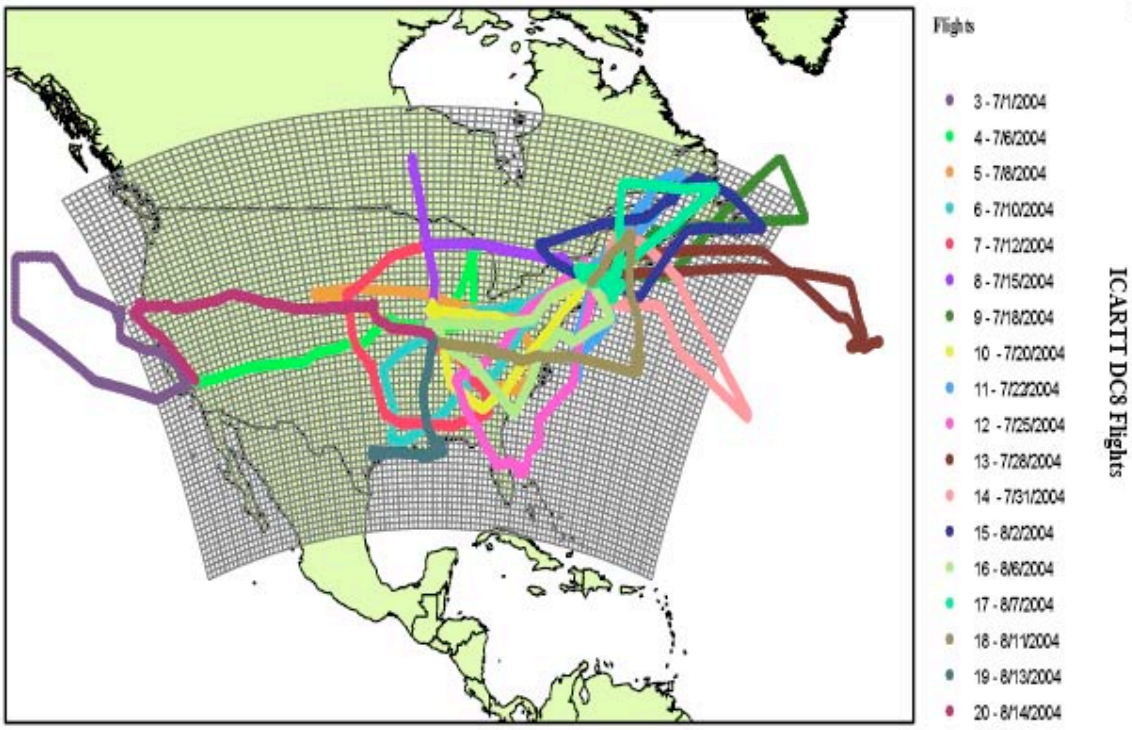

Figure 1. Color-coded map of all DC-8 flight tracks for INTEX-NA superimposed on the STEM 60 km model domain grid.

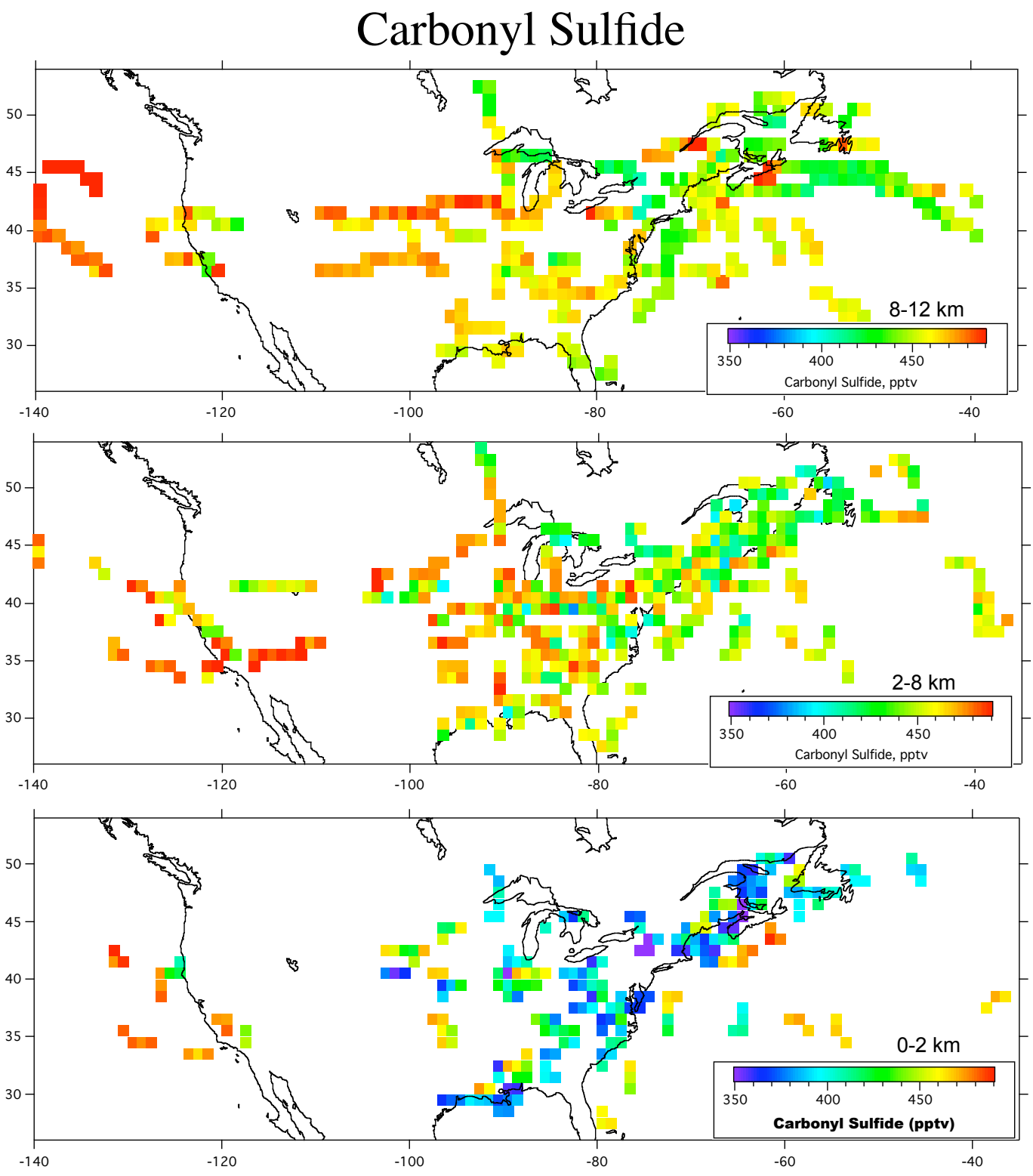

Figure 2. Map of 1°x1° mean observed OCS concentrations for 3 altitude ranges for all INTEX-NA DC-8 flights (July and August 2004).

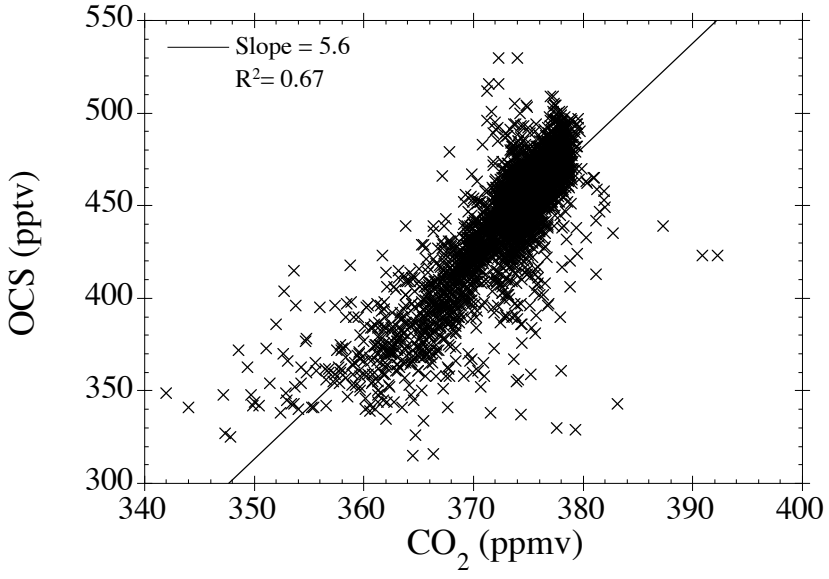

Figure 3. Correlation plot of OCS versus CO_2 for all for all INTEX-NA DC-8 flights (July and August 2004).

Date	Flight	R^2	Slope	Intercept
18-Jul	9	0.01	8	369
31-Jul	14	0.03	23	365
1-Jul	3	0.14	45	356
6-Jul	4	0.32	37	360
12-Jul	7	0.33	113	324
2-Aug	15	0.46	70	340
28-Jul	13	0.55	56	350
15-Jul	8	0.55	83	336
6-Aug	16	0.62	106	326
14-Aug	20	0.64	139	311
10-Jul	6	0.67	109	326
7-Aug	17	0.71	100	329
8-Jul	5	0.74	139	311
20-Jul	10	0.77	183	290
22-Jul	11	0.83	132	314
13-Aug	19	0.86	130	314
11-Aug	18	0.90	153	304
25-Jul	12	0.92	187	290

Table 1. Correlations of INTEX-NA observations of OCS and CO_2 for each DC-8 flight, sorted by R^2.

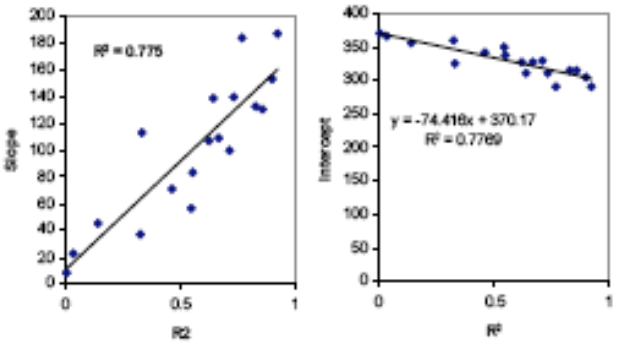

Figure 4. Correlation plots of R^2 values for CO_2 vs. OCS from Table 1 against CO_2 vs. OCS slopes and intercepts from Table 1.

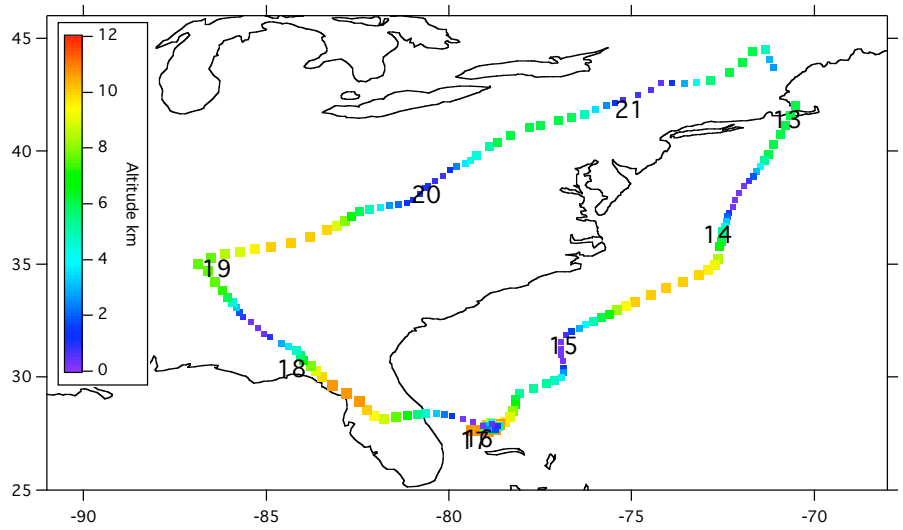

Figure 5. Flight track with color-coded altitude for INTEX-NA DC-8 Flight 12, July 25, 2004. Small blue squares correspond to the 6 BL runs. Black numbers correspond to UTC hour.

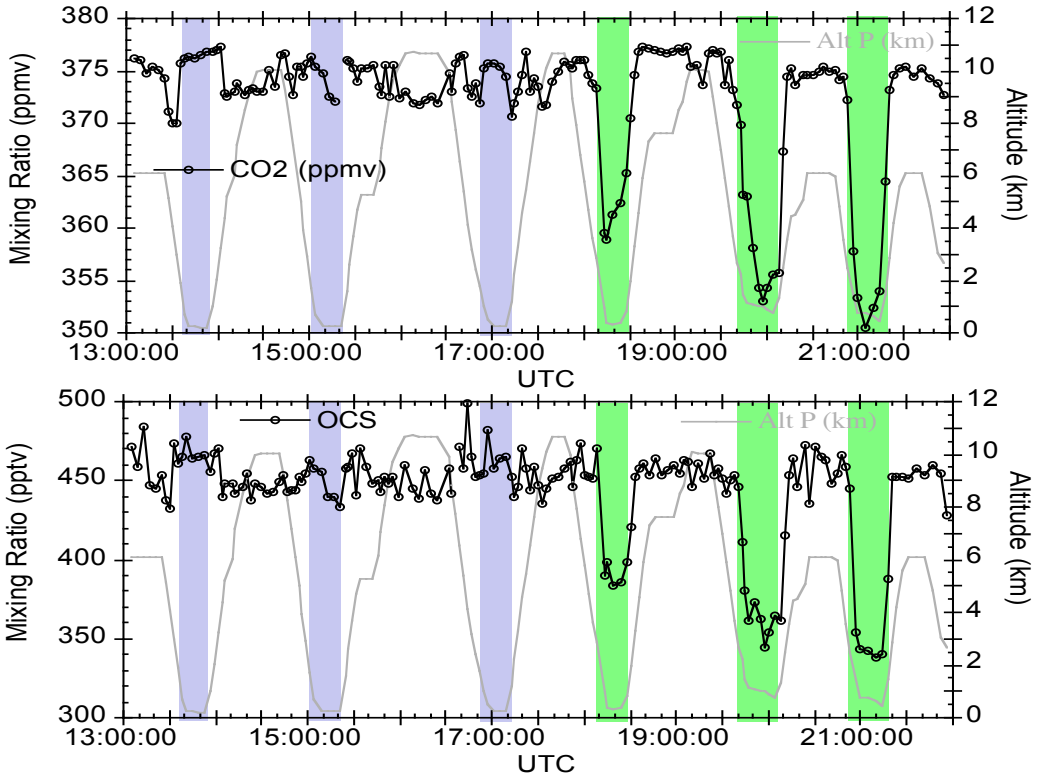

Figure 6. Mixing ratios of OCS and CO_2 and altitude vs. UTC hour for INTEX-NA DC-8 Flight 12, July 25, 2004. Blue shading highlights marine boundary layer legs and green shading highlights continental boundary layer legs.

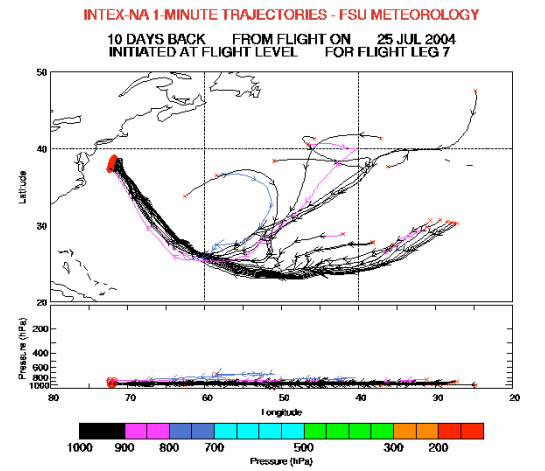

Figure 7. Backwards trajectory for the 1st low altitude leg during Flight 12, flown at about UTC hour 13:10 to 13:25.

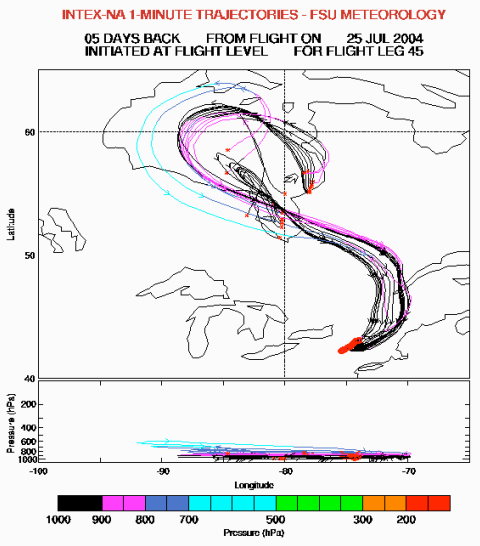

Figure 8. Backwards trajectory for the 5th low altitude leg during Flight 12, flown at about UTC hour 19:45 to 20:15.

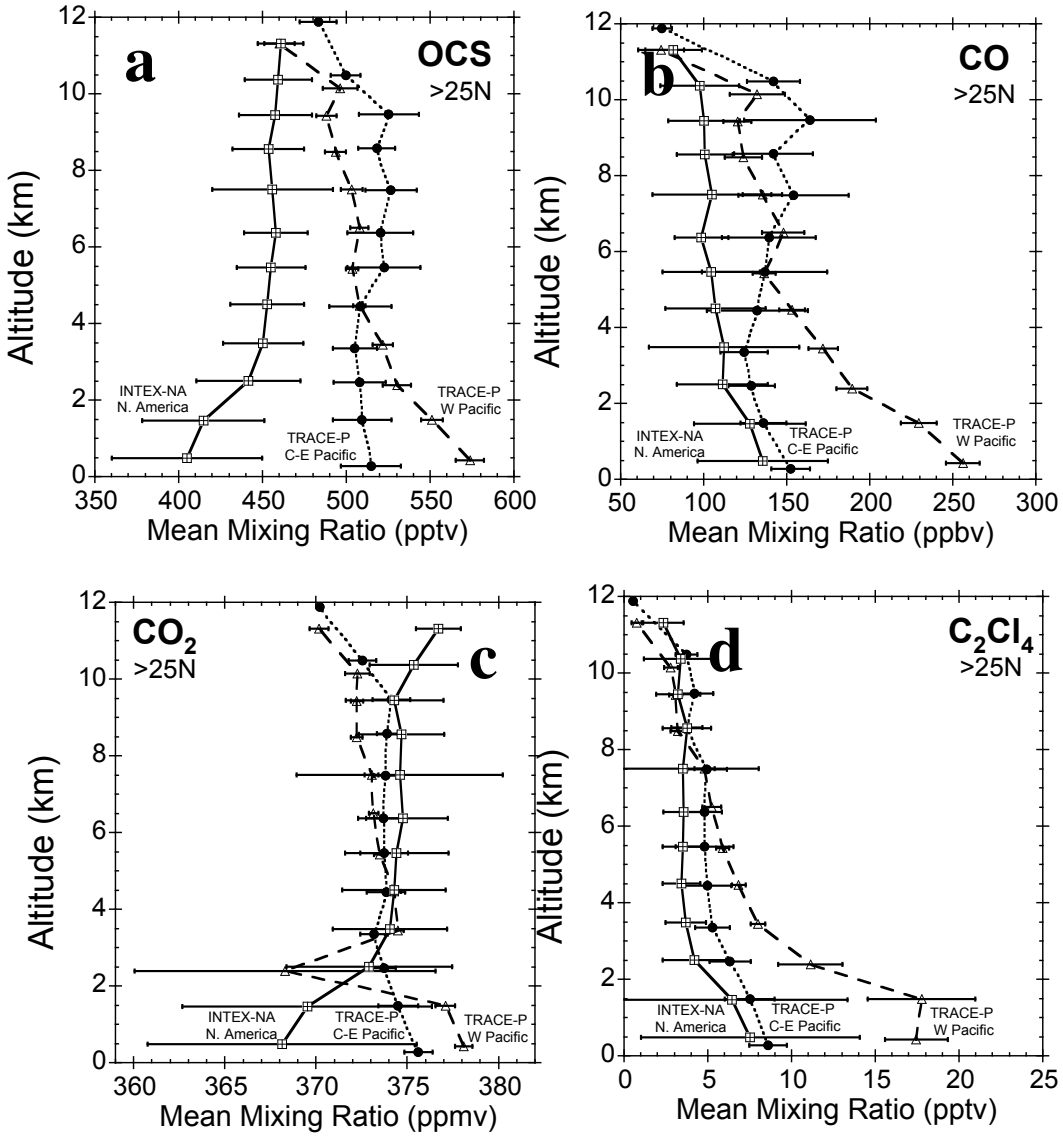

Figure 9. Mean (1-km increments) vertical profiles for a) OCS, b) CO, d) CO_2, d) C_2Cl_4. The mean values for INTEX-NA are compared to data collected over the Western Pacific (<165°E) and Central/Eastern Pacific (165°E-230°E) during TRACE P. Error bars represent 1 standard deviation from the mean.

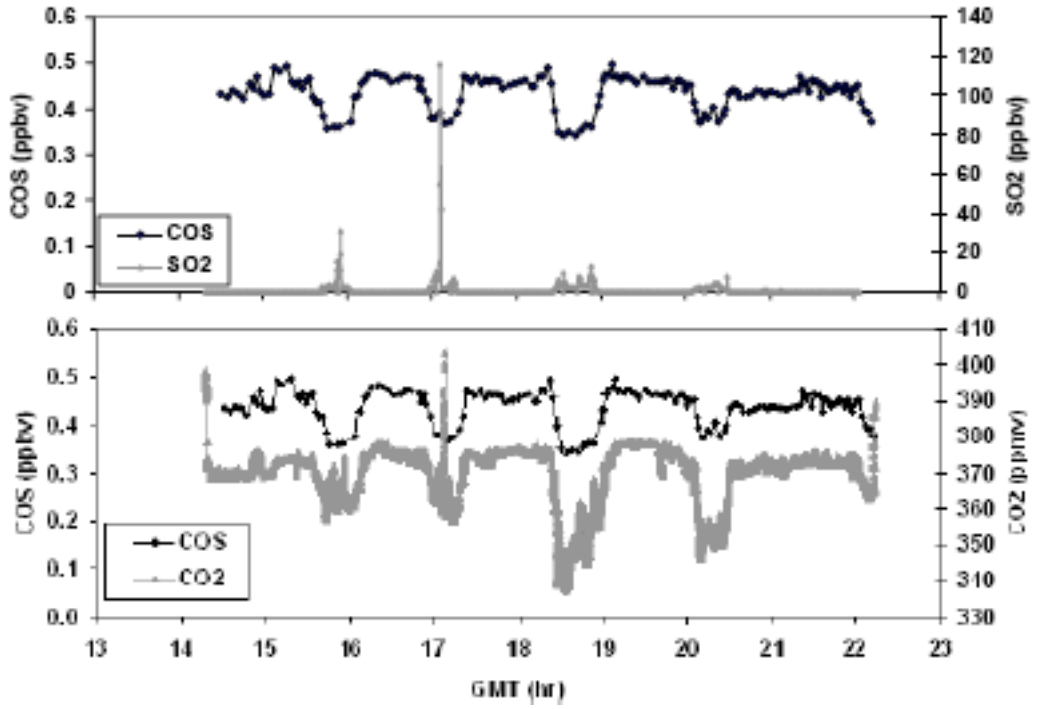

Figure 10. Time series for INTEX-NA DC-8 observations of OCS, SO_2, and CO_2 during Flight 12, July 20, 2004.

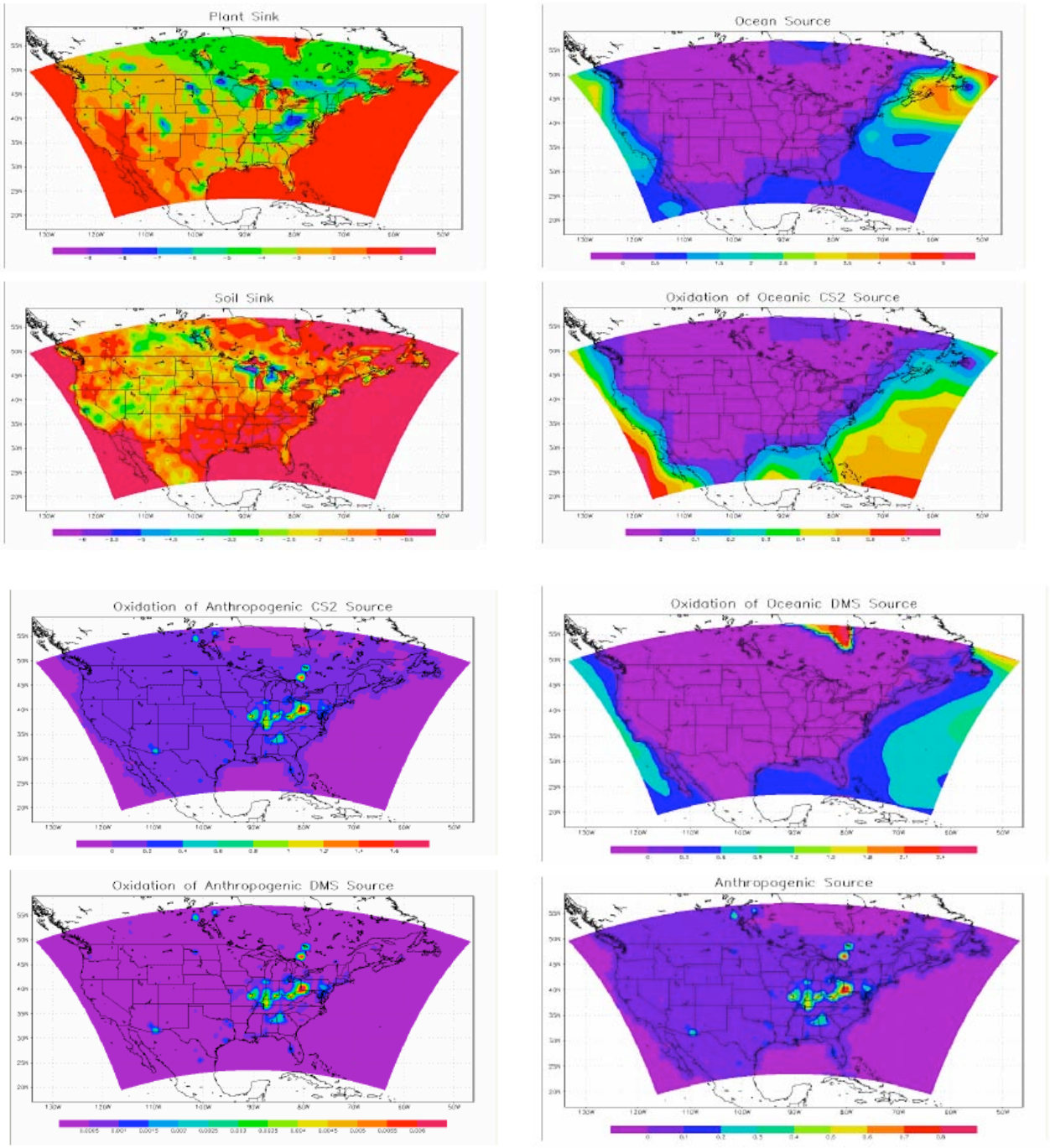

Figure 11. OCS surface fluxes interpolated from *Kettle et al.* [2002] to the STEM 60 km model domain.

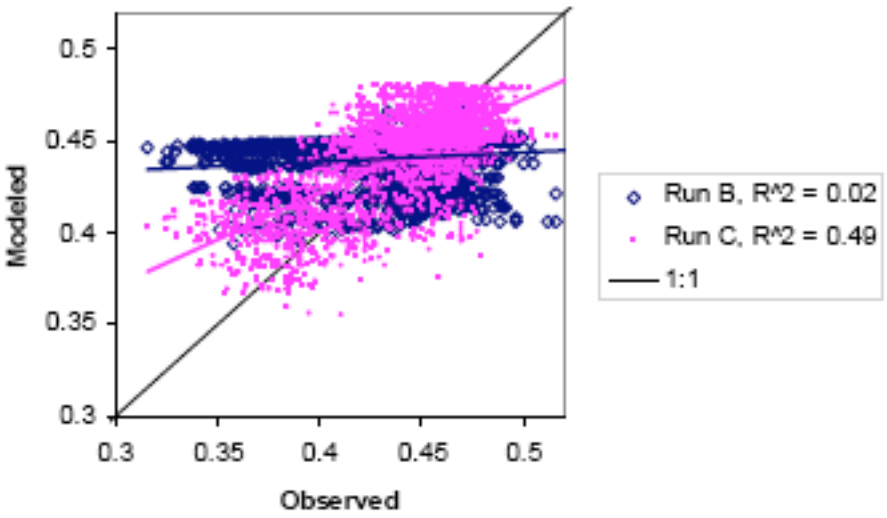

Figure 12a. OCS model vs. observed correlations for run B (blue) and run C (pink).

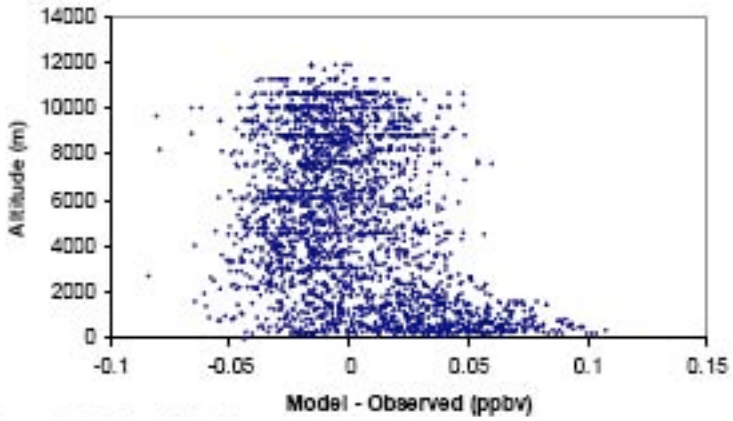

Figure 12b. OCS model vs. observed error for model run A.

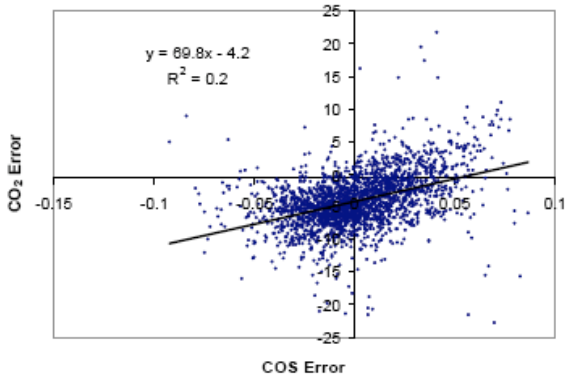

Figure 12c. Model error (model vs. observations) for OCS and CO_2 for all INTEX-NA DC-8 flights.

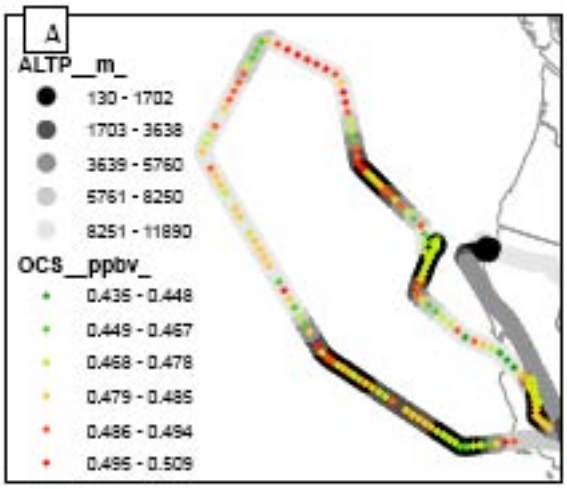

Figure 13. Observed OCS mixing ratios for Flight 3, July 1, 2004

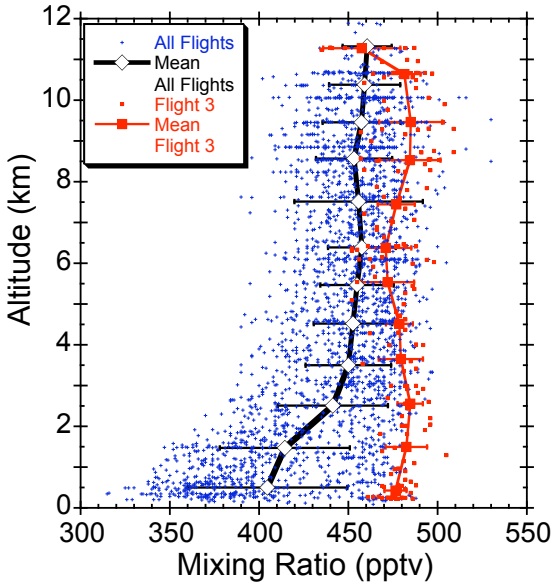

Figure 14. Observed OCS mixing ratios (blue) and 1-km mean values (black) for all flights for INTEX-NA. Samples from Flight 3, July 1, 2004, and 1-km mean values from this flight are highlighted in red.

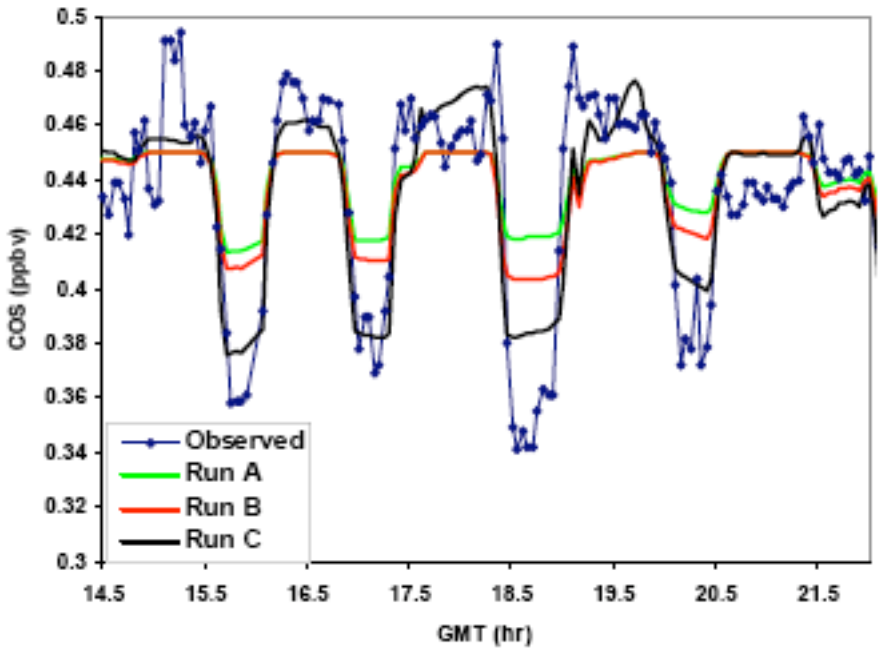

Figure 15. OCS concentrations from observed data and model runs A, B and C (see Table 2) for INTEX-NA DC-8 flight, July 20, 2004 (Flight 10).

Run	Surface Flux	Boundary Conditions	Mod–Obs (Avg/StDev)
A	Plant	Fixed 0.45 ppbv	
B	Plant + Other	Fixed 0.45 ppbv	0.0031/0.029
C	Plant*2 + Other	0.48 on western boundary; otherwise 0.45	0.0017/0.025

Table 2. Preliminary STEM OCS simulation.